Volume 17, Number 3, 2024. pp. 273-282

Jordan Journal of Physics

ARTICLE

A Study of the Abundance of Aluminium in Massive Stars

Alaa I. Abdallah and **N. M. Ershaidat**

Physics Department, The University of Jordan, Amman, 11942, Jordan.

Doi: **https://doi.org/10.47011/17.3.2**

Received on: 15/03/2022; *Accepted on: 02/03/2023*

Abstract: This study presents the results of the calculation of the mass fractions of isotopes from hydrogen to nickel during the entire core burning phases of a 25 $M_{\odot}$ star. A simple stellar model was used, considering four main parameters: temperature, density, initial composition, and time, without accounting for mass loss or mixing. The mass fractions of the isotopes were calculated using the open-source package NucNet Tools and the updated reaction rates from the JINA Reaclib database. A comparison of our results with existing similar data is performed and acceptable agreement is conspicuous. Hydrodynamic conditions in massive stars favor the production of ^{26}Al, therefore particular attention was given to the isotopes ^{26}Al and ^{27}Al and the ratio of their mass fractions R_{Al} for comparison with the literature. The averaged value of the controversial R_{Al} during the star's lifetime is found to be 1.68×10^{-4}.

Keywords: Elemental abundances in stars, Evolution, Stellar, Nuclear astrophysics, Hydrostatic stellar nucleosynthesis, Nucleosynthesis: stellar, Stars formation.

PACS: 97.10.Tk, 87.23.-n, 97.10.Cv, 26.20.-f, 7.10.Cv, 97.10.Bt.

Introduction

The study of massive stars plays a significant role in the advancement of theories dealing with the evolution of the universe. Stars with main-sequence masses of 20-25 $M_{\odot}$ are crucial sites of nucleosynthesis because they produce elements up to the iron peak in reasonable agreement with solar abundance ratios [1]. Rates of nucleosynthesis are high in these massive luminous stars. The synthesis of low Z elements, especially those with atomic numbers 8 to 20 is generally attributed to stars having masses greater than 10 $M_{\odot}$ [2]. Aluminium-26 is significantly produced with an initial mass above ~2 $M_{\odot}$ by proton capture on ^{25}Mg during core and shell hydrogen burning in all stars. In massive stars, additional phases of carbon and neon convective shell burning contribute to ^{26}Al production [3, 4]. Such stars end their lives as supernovae with the explosive ejection and explosive processing of their ashes from previous helium, carbon, neon, oxygen, and silicon burning phases [2]. Studying the elemental composition of stars and galaxies is crucial for understanding the origin and evolution of the universe. The abundance of an element is defined as the relative elemental content in a given system (e.g., the sun, a planet, a meteorite, or a comet). It can be determined by the mass fraction of that element relative to the total mass of the star. The sun, being the nearest star to us, is the best-known reference for abundance analyses of other stars. Solar system abundances are derived from the outer layers of the sun and meteorites [5, 6].

Aluminium is the 12th most abundant element in the universe. Amongst its 21 known isotopes, ^{27}Al is the only stable one, while ^{26}Al is non-stable with a half-life of 0.7 Myr. ^{26}Al and ^{27}Al

Corresponding Author: N. M. Ershaidat **Email**: n.ershaidat@ju.edu.jo

are synthesized from magnesium isotopes through the MgAl cycle reactions. The main production reaction is $^{25}Mg(p,\gamma)^{26}Al$ with ^{25}Mg produced by the neutron capture reaction: $^{24}Mg(n,\gamma)^{25}Mg$. It transforms almost all available ^{25}Mg into ^{26}Al. About 80% of the created ^{26}Al is in the ground state $^{26}Al^{g}$, while the remaining 20% exists in the isomeric state $^{26}Al^{i}$ which disintegrates in 6.3 s into ^{26}Mg [7].

Aluminium-26 is an important isotope because it plays a key role in γ-ray astronomy and cosmochemistry [8]. Since the lifetime of this nucleus is very short compared to the time scale of galactic evolution, it offers an opportunity to confront nucleosynthesis theories with observational data [9]. Interest in ^{26}Al increased following the discovery that this nuclide decays into various meteoritic inclusions, leading to an observed ^{26}Mg excess, known as the Mg anomaly[1]. This anomaly indicates that the measured isotopic ratio of magnesium cannot be related to the solar composition of the given element [10]. This is compatible with an average abundance ratio of $^{26}Al/^{27}Al \simeq 5\times10^{-5}$ at the time of formation of the solar system.

Interest in ^{26}Al was further amplified by the discovery of the 1.8 MeV γ-ray line, which is produced in beta decay of ^{26}Al. The disciplines of gamma-ray astronomy and nuclear astrophysics are brought closer together because of this particular line. Based on the intensity of this line, it is estimated that about 3-4 $M_{\odot}$ of ^{26}Al nuclides are present in the interstellar medium of our galaxy. This discovery has provided insight into the possible astrophysical sources of ^{26}Al and their distribution throughout the galaxy [11, 12].

The synthesis of aluminum can occur in various astrophysical sites: 1) during the burning phases of stellar evolution, e.g., massive main sequence stars, 2) in asymptotic giant branch stars, and 3) in explosive and non-explosive burning events, e.g., supernovae and novae [11].

[1] This anomaly can be explained as the result of the bombardment of a gas of solar composition by high fluxes of energetic protons. It follows that ^{26}Mg is mainly created and stored in the form of ^{26}Al by the reaction ^{26}Mg (p, n)^{26}Al. The beta decay of ^{26}Al restores ^{26}Mg. Aluminum-rich materials condensing in meteorites have positive ^{26}Mg anomalies, whereas magnesium-rich materials have negative anomalies [10].

The production and destruction reaction rates of ^{26}Al depend on the different temperature and density regimes of these corresponding astrophysical sites. Theoretical calculations have determined uncertainties for some of these reactions, but others couldn't be calculated because of a lack of information. This is mainly due to experimental uncertainties in measuring expected low-energy resonances in proton decay [13].

Earlier work on computing the abundance of $^{26}Al/^{27}Al$ in massive stars has been done by several authors. Wallerstein *et al*. calculated the time evolution of the mass fractions of the MgAl chain reactions at temperatures ~ 0.05 GK, assuming a constant density of 100 g cm^{-3} and solar initial abundances [14]. They found that the mass fraction of ^{26}Al is on the order of 10^{-6}, while the mass fraction of ^{27}Al is around 6×10^{-4} during 10^{10} s. They concluded that the main effect of the MgAl cycle at low temperatures is the production of ^{26}Al at the expense of ^{25}Mg, which also leads to the production of ^{26}Mg via the β^{+} decay of ^{26}Al. High $^{26}Al/^{27}Al$ ratios (0.38-0.95) were achieved, with uncertainty in this ratio attributed to the uncertainty in the $^{26}Mg(p,\gamma)^{27}Al$ and $^{26}Al(p,\gamma)^{27}Si$ reaction rates. For higher temperatures, Wallerstein *et al*. performed the calculations at a constant temperature of 0.3 GK and density of 6×10^{3}g cm^{-3}. These conditions might be found at the peak of a nova explosion on an O-Ne white dwarf. The mass fractions of ^{26}Al and ^{27}Al were found to be in the range of 10^{-6}-10^{-5} and 10^{-5}-10^{-4} during 10^{3} s, respectively. They concluded that ^{26}Al evolves in parallel with ^{25}Mg, and the drop in ^{24}Mg diminishes the production of ^{25}Mg, resulting in a decrease in both ^{25}Mg and ^{26}Al. The ^{27}Al mass fraction shows the effects of competition between the $^{26}Mg(p,\gamma)^{27}Al$ reaction and the $^{27}Al(p,\gamma)^{28}Si$ and $^{27}Al(p,\alpha)^{24}Mg$ reactions [14].

Nucleosynthesis occurring in the carbon shell of a massive star ($M_{\star}$= 12 $M_{\odot}$), with emphasis on the production of ^{26}Al, is studied by Arnett and Wefel [15]. They used an over-simplified model for their chosen star, with a temperature greater than 2 GK and a density of 10^{5}g cm^{-3}. They found that the $^{26}Al/^{27}Al$ ratio is approximately (1-2) × 10^{-3} [15].

Iliadis studied the nucleosynthesis of isotopes produced during the burning phases of a 25 $M_{\odot}$ with solar initial composition as per Lodders [6].

The calculations were performed using a post-processing reaction network that requires constant temperature, density, time, and initial composition. The used network is not available publicly. Using their reaction rates, Iliadis *et al*. obtained the mass fractions of the isotopes during the advanced burning phases [16, 17].

In this work, the mass fractions (abundances) of isotopes (H to Ni) were calculated using a similar simple model but with updated reaction rates from the JINA Reaclib database for a 25 $M_{\odot}$ star. This was done for comparison purposes with the results of Iliadis [17]. The $^{26}Al/^{27}Al$ ratio was also calculated and compared to findings from previous studies.

Methodology

A nuclear reaction network is a set of reactions between nuclear species that leads to the production and destruction of elements. Abundances can be calculated by solving a system of coupled equations, the so-called Bateman equations, using specific temperature and density as initial conditions. The open-source package "NucNet Tools", developed by the Webnucleo project headed by Bradley Meyer from the Astronomy and Astrophysics group at Clemson University, South Carolina, USA, is used to compute the abundances of a selection of isotopes ranging from H to Ni [18, 19]. NucNet Tools uses the Newton-Raphson method to iteratively solve these equations until a defined convergence is reached. The procedure is detailed and well explained by Meyer [20].

In this work, the nucleosynthesis of elements from H to Ni, in a $25M_{\odot}$ star is studied. Such a star undergoes six burning phases: hydrogen burning, helium burning, carbon burning, neon burning, oxygen burning, and silicon burning.

A simple model was used to obtain the abundance of the mentioned isotopes, utilizing parameters such as temperature, density, initial composition, and the lifetime needed for each stage to burn its content. This simple model is aligned with the parameters used by Iliadis [17] for comparison purposes.

The main parameters used for initializing the calculations - temperature and density - depend on the expansion timescale τ, which can be defined as $\frac{1}{\tau} = -\frac{1}{\rho}\frac{\partial \rho}{\partial t}$. By choosing τ to be infinity, the core temperature and density, expressed as $T(t) = T(0)\ e^{-t/\tau}$ and $\rho(t) = \rho(0)\ e^{-t/\tau}$, are kept constant all along the calculations. These static calculations for such a star with solar initial composition have been performed using NucNet Tools [6].

This assumption is representative of the hydrostatic status of the core during the burning phases. Although this does not represent a real star, it is useful for obtaining physical insights into nucleosynthesis and energy production.

The initial abundances of the isotopes for core hydrogen burning were taken from Lodders' solar composition data [6]. The final values of abundances of each phase (ashes), resulting from the solution of coupled equations, served as the initial abundances for the next phase.

Appropriate nuclides and reaction data from the JINA (Joint Institute for Nuclear Astrophysics) database were used to obtain the reaction rates of the isotopes [21].

Calculations for each of the six burning phases, mentioned earlier, were performed using the initial conditions of temperature, density, and lifetime, as shown in Table 1. These conditions are similar to those used by Iliadis [17] and Woosley *et al*., 2002 [22].

TABLE 1. Initial conditions for the core burning phases.

Burning Phase	Temperature (GK)	Density (g cm^{-3})	Phase Duration
Hydrogen	0.0381	3.81	6.7 Myr
Helium	0.196	7.6×10^{2}	0.839 Myr
Carbon	0.9	1×10^{5}	3.2 kyr
Neon	1.5	5×10^{6}	0.891 yr
Oxygen	2.2	3×10^{6}	0.412 yr
Silicon	3.6	3×10^{7}	0.733 yr

Results and Discussion

For clarity, calculations are arranged by burning phase containing the discussion of the properties and the results of each single phase. The special case of aluminum isotopes is treated in detail at the end of this section.

Hydrogen Burning

In this first phase, hydrogen burns to produce helium via the proton-proton (pp) chains and the carbon-nitrogen-oxygen (CNO) cycles. The star now is in its main sequence phase and will continue burning hydrogen for approximately 6.7 Myr. Initially, the star is predicted to contain 0.7491 hydrogen, 0.2377 helium, and 0.0133 metals (elements heavier than helium). Calculations for the first phase were performed at T = 0.0381 GK (denoted as t_9 = T in GK in the following sections) and $\rho = 3.81$ g cm^{-3}.

The mass fraction of the produced helium reaches the value of 0.985, and the calculation is terminated when the mass fraction of hydrogen decreases to 2.73×10^{-5}. The main product of this phase is ^{4}He, and most of the initial ^{12}C and ^{16}O are converted to ^{14}N during the CNO burning. The time evolution of the mass fractions of ^{1}H, ^{4}He, ^{12}C, ^{13}C, ^{14}N, ^{16}O, ^{17}O, and ^{18}O during core hydrogen burning is shown in Fig. 1.

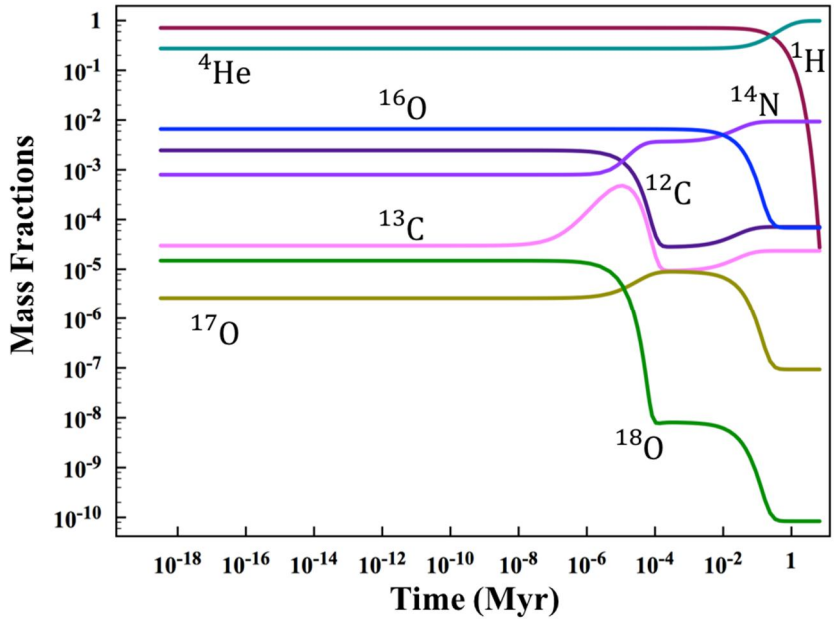

FIG. 1. Time evolution of the mass fractions during core hydrogen burning. Hydrogen isotopes are sufficiently transformed into ^{4}He isotopes, which accumulate in the core to initiate the next burning phase. The calculations are terminated when hydrogen mass fractions fall below 2.73×10^{-5}.

Helium Burning

Once hydrogen is exhausted inside the core, leaving helium as the product of the previous burning phase, the core's temperature rises to around 0.1 GK, initiating helium burning. Meanwhile, hydrogen burning continues in a shell around the core. The star now moves to the next phase, the so-called red supergiant phase, where helium is transformed into heavier elements over approximately 0.839 Myr. The calculations were conducted at 0.196 GK and 0.76×10^{3} g cm^{-3}. The final mass fractions from the end of the hydrogen-burning phase were used as initial values for helium burning. The mass fraction of helium after the burning decreases to 0.006, while the mass fractions of carbon and oxygen increase to 0.308, and 0.667, respectively. The core becomes composed of carbon and oxygen, which are the main products of this phase. Figure 2 shows the time evolution of the mass fractions of ^{4}He, ^{12}C, ^{16}O, ^{20}Ne, ^{24}Mg, ^{25}Mg, and ^{26}Mg during core helium burning. The most abundant nuclides at the end of the calculation are ^{12}C (0.3075), ^{16}O (0.6671), and ^{20}Ne (0.0141). The mass fractions of the other isotopes are less than 10^{-3}.

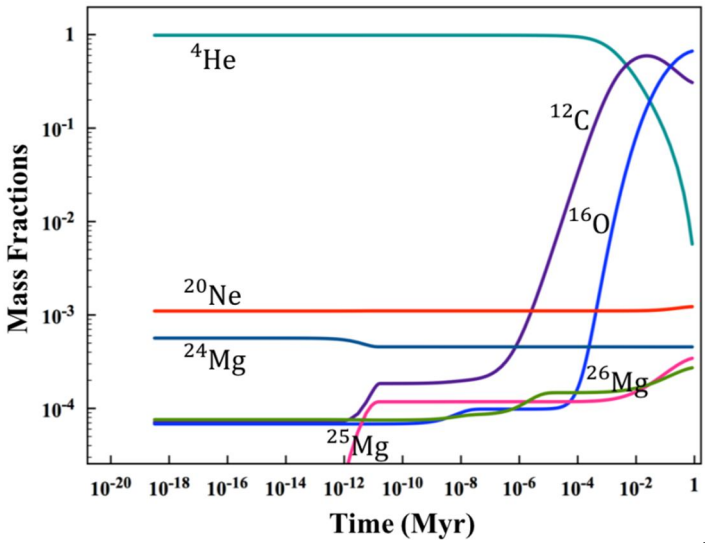

FIG. 2. Time evolution of the mass fractions during core helium burning. In this phase, ^{4}He is transformed into ^{12}C and ^{16}O, which become the main fuel for the carbon-burning phase. The calculations are terminated when the mass fraction of helium reaches 0.006. The mass fractions of carbon and oxygen increase to 0.308, and 0.667, respectively.

Carbon Burning

At the end of the helium-burning phase, the mass fraction of helium decreases by a factor of nearly 100, and the core becomes composed of carbon and oxygen. The temperature rises to around 0.9 GK where carbon burning begins, and helium burning continues in a shell around the core. During the burning, the existing free α particles, protons, and neutrons interact with the nuclei present, including CNO nuclei from the hydrogen- and helium-burning phases, leading to the production of heavier elements.

At the end of the calculation, the mass fraction of carbon decreases to 0.004, while the mass fractions of oxygen and neon increase to 0.497, and 0.409, respectively. Figure 3 shows the time evolution of the mass fractions of ^{12}C, ^{16}O, ^{20}Ne, ^{21}Ne, ^{22}Ne, ^{23}Na, ^{24}Mg, ^{25}Mg, ^{26}Mg, and ^{27}Al during core carbon burning. The most abundant nuclides at the end of the calculation are ^{16}O (0.497), ^{20}Ne (0.409), ^{23}Na (0.023), ^{24}Mg (0.040), and ^{25}Mg (0.011). The other isotopes have mass fractions less than 10^{-3}. Results for the main isotopes, ^{16}O and ^{20}Ne, agree rather well with previous studies, showing values of 0.600 and 0.350, respectively [17].

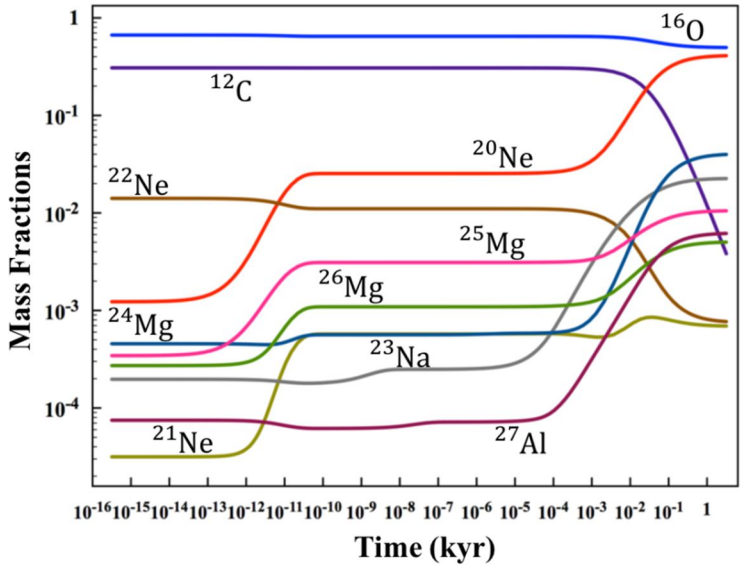

FIG. 3. Time evolution of the mass fractions during core carbon burning. The main fuel in this phase is ^{12}C and it burns to produce ^{16}O and ^{20}Ne, which are needed for the next burning phase. The mass fraction of carbon decreased to 0.004, while the mass fractions of oxygen and neon increased to 0.497, and 0.409, respectively.

Neon Burning

Neon burning starts with the reaction ^{20}Ne (γ, α) ^{16}O when the central temperature t_9 = 1.5 and the density ρ = 5×10^6 g cm^{-3}. This temperature is enough to photodisintegrate ^{20}Ne, and the freed α particles can combine readily with ^{20}Ne to form ^{24}Mg. The main products of this phase are ^{16}O, ^{24}Mg, and ^{28}Si. Figure 4 shows the time evolution of the mass fractions of ^{16}O, ^{20}Ne, ^{24}Mg, ^{25}Mg, ^{26}Mg, ^{27}Al, ^{28}Si, ^{29}Si, and ^{30}Si during core neon burning. The most abundant nuclides at the end of the calculation are ^{16}O (0.708), ^{24}Mg (0.115), ^{27}Al (0.015), ^{28}Si (0.112), ^{29}Si (0.015), and ^{30}Si (0.013). The mass fractions of ^{16}O and ^{24}Mg agree with the values reported in [17]: 0.770 and 0.110, respectively.

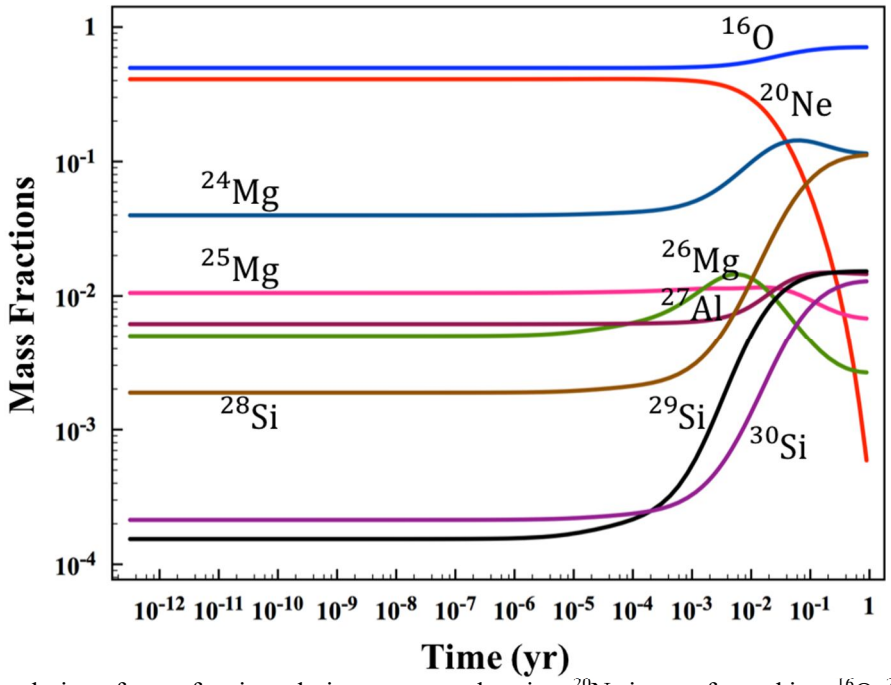

FIG. 4. Time evolution of mass fractions during core neon burning. ^{20}Ne is transformed into ^{16}O, ^{24}Mg, and ^{28}Si, preparing the with fuel for the subsequent oxygen burning.

Oxygen Burning

Oxygen burning begins when the core temperature rises to around 2.2 GK, while neon continues burning in a shell around the core. The oxygen nuclei begin to fuse together, producing ^{28}Si and α particles. Several reactions occur, freeing α particles, protons, and neutrons that interact with the present nuclei and produce heavier elements. The main isotopes resulting from this phase are ^{28}Si and ^{32}S. Figure 5 shows the time evolution of the mass fractions of ^{16}O, ^{27}Al, ^{28}Si, ^{29}Si, ^{30}Si, ^{31}P, ^{32}S, ^{33}S ^{34}S, ^{35}Cl, and ^{36}Ar during core oxygen burning at a constant temperature t_9 = 2.2 and density ρ = 3×10^{6}g cm^{-3}. The most abundant nuclides at the end of the calculation are ^{28}Si (0.565), ^{32}S (0.299), ^{34}S (0.031), and ^{36}Ar (0.028). These abundances agree rather well with the corresponding values in [17]: ^{28}Si (0.54), ^{32}S (0.280), ^{34}S (0.044), and ^{36}Ar (0.027). For all other isotopes, calculations give mass fractions less than 10^{-3}.

Silicon Burning

At the end of the oxygen-burning phase, the mass fraction of oxygen decreases, and the core becomes composed of silicon and sulfur. The temperature rises to around 3.6 GK, where silicon burning begins, while oxygen-burning continues in a shell around the core. This phase involves a series of nuclear reactions that start with the products of the oxygen burning and synthesize nuclei up to the iron peak. Photodisintegration of the nuclei produces α particles, protons, and neutrons, which are essential for this synthesis. Figure 6 shows the time evolution of the mass fractions of ^{24}Mg, ^{27}Al, ^{28}Si, ^{29}Si, ^{30}Si, ^{32}S, ^{34}S, ^{36}Ar, ^{52}Cr, ^{53}Mn, ^{54}Fe, ^{55}Fe, ^{56}Fe, ^{57}Co, and ^{58}Ni during core silicon burning. The calculation assumes a constant temperature t_9 = 3.6 and density ρ = 3×10^7 g cm^{-3}. The most abundant nuclides at the end of the calculation are ^{52}Cr (0.008), ^{53}Mn (0.018), ^{54}Fe (0.683), ^{55}Fe (0.047), ^{56}Fe (0.081),

^{57}Co (0.020), and ^{58}Ni (0.103). These values do not agree with those reported in [17]. The mass fractions of the other isotopes are found to be less than 10^{-4}.

At the end of this phase, the core will be composed of iron. Since iron nuclei are the most stable nuclei, the core will collapse into a neutron star and release an enormous amount of energy. A tiny fraction of this energy is sufficient to explode the star as a supernova [21].

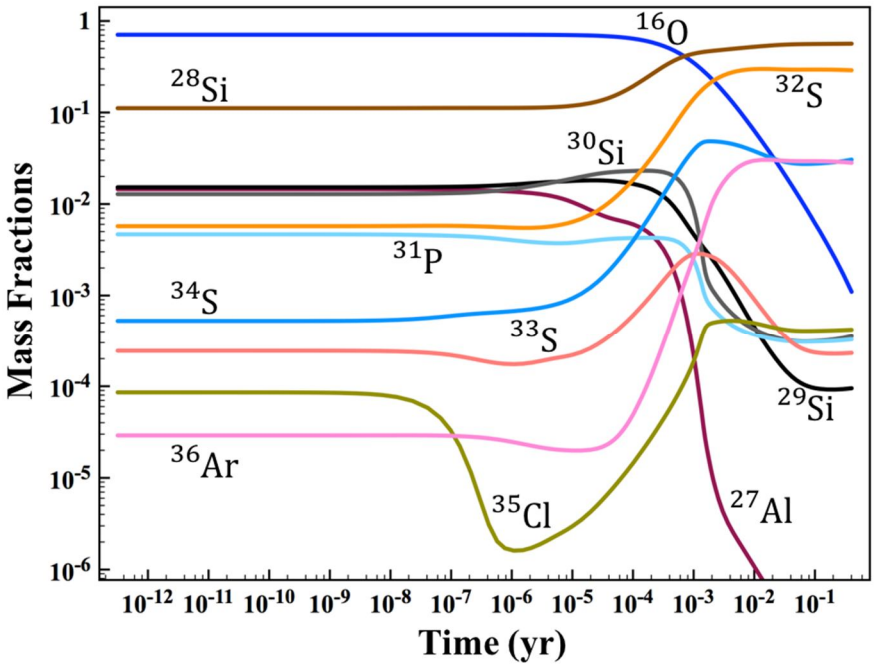

FIG. 5. Time evolution of the mass fractions during core oxygen burning. The mass fraction of oxygen decreases to 0.001, while the mass fractions of ^{28}Si and ^{32}S increase to 0.565 and 0.290, respectively, preparing them for the silicon burning phase.

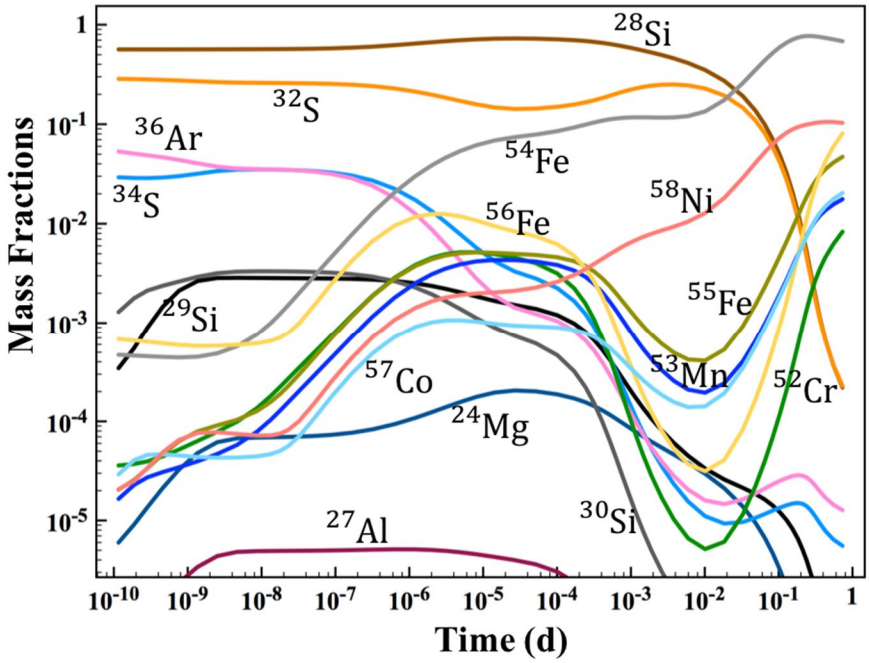

FIG. 6. Time evolution of the mass fractions during core silicon burning. Si nuclei burn to produce heavier elements (up to the iron peak). Iron isotopes cannot undergo further fusion, they rather let the core collapse to a neutron star and release an enormous amount of energy. The star now starts to explode as a supernova.

^{26}Al and ^{27}Al

Detailed calculations were performed for the mass fractions of ^{26}Al and ^{27}Al and the ratio R_{Al} was defined as:

$$R_{Al} = \frac{mass\ fraction\ of\ ^{26}Al}{mass\ fraction\ of\ ^{27}Al} \quad (1)$$

The production and destruction of aluminum isotopes come from several reactions, including proton-induced, neutron-induced, α-induced, and photodisintegration reactions. Figures 7 and 8 show the time evolution of the mass fractions of ^{26}Al and ^{27}Al and the variation with of their mass fractions ratio during the advanced burning phases, respectively.

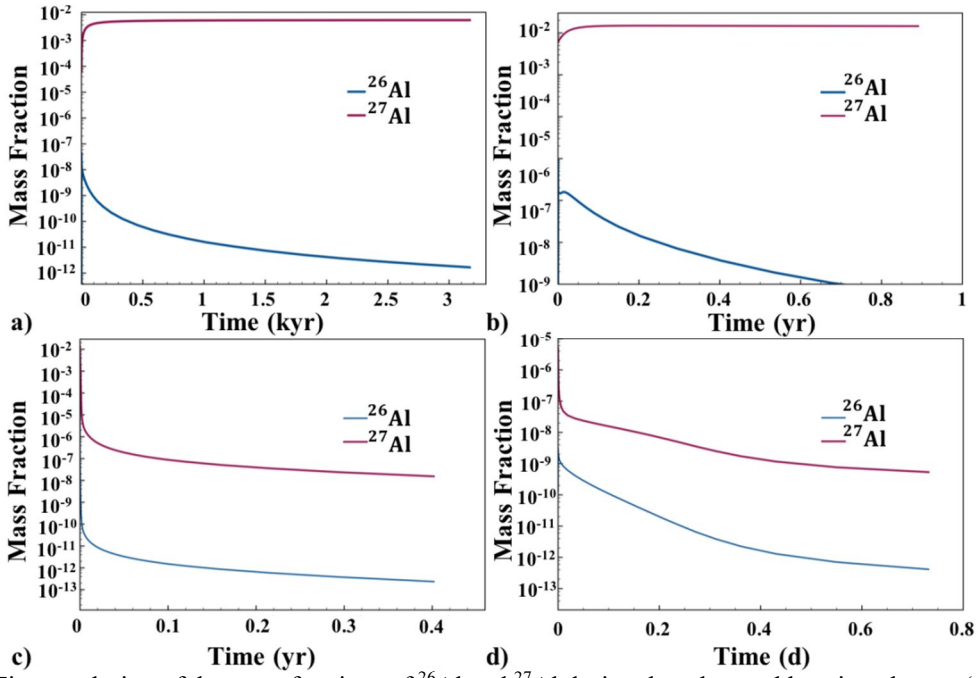

FIG. 7. Time evolution of the mass fractions of ^{26}Al and ^{27}Al during the advanced burning phases: (a) carbon burning (b) neon burning, (c) oxygen burning, and (d) silicon burning. It is concluded that ^{26}Al has high destruction reaction rates, and the reaction rate of ^{26}Mg(p, γ)^{27}Al is higher than the reaction ^{25}Mg(p, γ)^{26}Al in these phases.

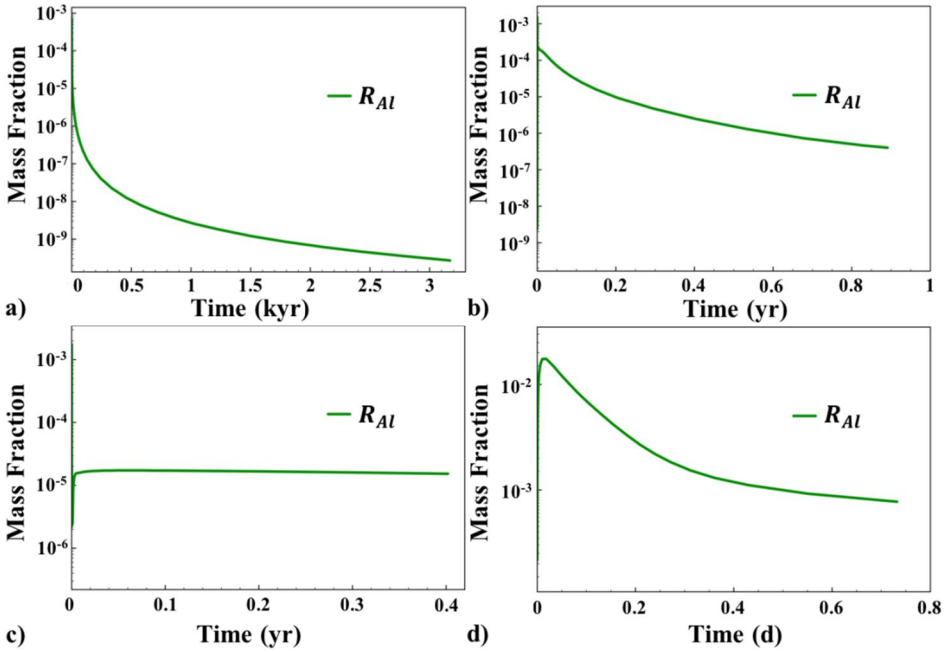

FIG. 8. The time variation of the mass fraction ratio ^{26}Al/^{27}Al during the burning phases: (a) carbon burning, (b) neon burning, (c) oxygen burning, and (d) silicon burning.

During the evolution of the star, the core evolves to a higher temperature where the production and destruction reaction rates increase [23]. We notice that at 0.9 GK, the required temperature for the core carbon burning phase, most of ^{26}Al is destroyed during the final two thousand years. This would also mean that the ratio R_{Al} should normally decrease, as shown in Fig. 8(a). When the temperature is around 1.5 GK, which is the required temperature for neon burning, the production and destruction reaction rates of both ^{26}Al and ^{27}Al indicate that the ratio R_{Al} should decrease during the major part of the phase, and this is what we observe in Fig. 8(b).

During oxygen burning, both isotopes are destructed, thus, R_{Al} decreases from its initial value, as shown in Fig. 8(c). In the final phase, an increase of the ratio R_{Al} is observed for the period of [0.001-0.05] d, followed by a decrease for the remainder of the phase, as seen in Fig. 8(d). A thorough study should consider the possible systematic and statistical errors.

Conclusions

The open-source package NucNet-tools from the Webnucleo group was used to calculate the mass fractions of isotopes from H to Ni in a 25 $M_{\odot}$ star across six burning phases: hydrogen, helium, carbon, neon, oxygen, and silicon (Figs.1-6). Special attention was given to the isotopes ^{26}Al and ^{27}Al. Comparisons were made with the results of Iliadis [17] for the advanced burning phases. The comparison shows a satisfactory agreement for the carbon, neon, and oxygen-burning phases. This is due to the fact that calculations for these phases have been performed with the same input physics using simple nuclear networks. However, differences were noted in the silicon burning phase. Iliadis [17] used different initial mass fractions for ^{28}Si and ^{30}Si, set at 0.70 and 0.30, respectively, while our calculations yielded 0.56 and 0.001, ashes of the oxygen-burning phase, respectively. These discrepancies can be attributed to differences in initial abundances, nuclear reaction networks involved, and reaction rates used in the calculations.

The average value of the calculated aluminum ratio, R_{Al}^{avg}, was found to be 2.85×10^{-4}, 2.23×10^{-4}, 1.29×10^{-4}, and 3.46×10^{-3} in carbon, neon, oxygen, and silicon burning phases, respectively. For the first three advanced phases, it was observed that as the temperature increases inside the core, the aluminum ratio R_{Al}^{avg} decreases. For the silicon burning phase, reactions favoring the production of both isotopes have higher reaction rates than the destruction ones, which explains the different behavior of the variation of R_{Al}, as seen in Fig. 8(d), hence the peculiar value of $R_{Al}^{avg} = 3.46\times10^{-3}$.

One way of testing the calculation procedure is to observe the time evolution of the mass fractions of the main fuels during the various core burning phases. As expected, the latter initially varies smoothly, followed by a more pronounced decrease during the later stages of each phase.

The results of this study are, hopefully, expected to provide new insights into nucleosynthesis and the evolution of massive stars.

Acknowledgment

The authors would like to thank Professor Bradley Meyer, Physics Department, Clemson University, SC, USA, and his students for sharing the open-source package NucNet Tools/Webnucleo project for solving some astrophysical problems.

References

[1] Nomoto, K. and Hashimoto, M., Phys. Rep., 1 (1988) 163.

[2] Woosley, S. and Weaver, T., ApJ, 238 (1980) 1017.

[3] Brinkman, H.E., Doherty, C.L., Pols, O.R., et al., ApJ, 884 (2019) 38

[4] Lemongi, M. and Chieffi, A., ApJ, 647 (2006) 483.

[5] Grevesse, N. and Sauval, A., IOP, 3 (2005).

[6] Lodders, K., ApJ, 591 (2003) 1220.

[7] Mowlavi, N. and Meynet, G., ApJ, 361 (2000) 959.

[8] Siess, L. and Arnould, M., A&A, 489 (2008) 395.

[9] Prantzos, N., AIP Conf. Proc., 232 (1991) 129.

[10] Kuroda, P.K. and Bakhtiar, S.N., GJ, 20 (1986) 311.

[11] Forestini, M., Arnould, M., and Paulus, G., A&A, 252 (1991) 597.

[12] Iliadis, C., Schange, T., Rolfs, C., et al., Nucl. Phys. A, 512 (1990) 509.

[13] Iliadis, C., D'auria, J.M., Starrfield, S., et al., ApJS, 134 (2001).

[14] Wallerstein, G., Icko Iben, Jr., Parker, P., et al., Rev. Mod. Phys., 69 (1997) 4.

[15] Arnett, W.D. and Wefel, J.P., ApJ, 224 (1978) L139.

[16] Iliadis, C., Longland, R., Champagne, A.E., et al., Nucl. Phys. A, 841 (2010) 31.

[17] Iliadis, C., "Nuclear Physics of Stars", 2nd Ed.., (John Wiley & Sons, Weinheim, 2015).

[18] Meyer, B.S., PoS. (NIC XII), 146 (2013) 096.

[19] Talafha, M., Al-Wardat, M., and Ershaidat, N., Astrophys. Bull., 73 (2018) 2.

[20] Meyer, B., "Webnucleo Technical Report: Network Calculations with lib-nucnet", (2011), http://libnucnet.sourceforge.net/pubs/technical_reports/2011-04-17-1.pdf.

[21] Cyburt, R., Amthor, A., Ferguson, R., et al., ApJS, 189 (2010) 240. (see also https://reaclib.jinaweb.org/index.php).

[22] Woosley, S., Heger, A., and Weaver, T., Rev. Mod. Phys., 74 (2002) 1015.

[23] LeBlanc, F., "An Introduction to Stellar Astrophysics", 1st Ed., (John Wiley & Sons, West Sussex, U.K, 2010).